Nulling Interferometry for Spectroscopic Investigation of Exoplanets - A Statistical Analysis of Imperfections

Oswald Wallner[a], Klaus Kudielka[b], Walter R. Leeb[a]

[a]Institut für Nachrichtentechnik und Hochfrequenztechnik, Technische Universität Wien, Austria
[b]Contraves Space AG, Zurich, Switzerland

ABSTRACT

In ESA's Infrared Space Interferometry mission, a multi-aperture interferometer fed by telescopes will serve to analyse exoplanets orbiting bright stars. Spectroscopy of the planet's radiation could give hints on the possibility of the existence of life. However, for a Sun/Earth-like constellation, a star light rejection ratio of some $80dB$ is required. This is the factor by which the star light is suppressed, when comparing the interferometer with a standard, wide-field-of-view telescope.

We investigate the nulling capability of space-based interferometers, realized either in fiber or bulk optics, in the presence of imperfections of the structure and of optical components. Mismatch of amplitude, optical path length, and polarization among the interferometer arms is taken into account, as well as multiple reflections and telescope imperfections. The parameters describing the interferometer's receive characteristic, which are actively controlled or influenced by environmental disturbances, are modeled stochastically.

We analyse Sun/Earth-like constellations by numerical simulation for a wavelength range of 6 to 18 microns. The expected value of the star light rejection ratio is calculated for several interferometer configurations. The exemplary numerical results confirm the extreme requirements for interferometer uniformity and give a quantitative insight into the dependence of the attainable rejection ratio on individual and/or combined interferometer imperfections.

Keywords: nulling interferometry, rejection ratio, imperfections, statistical analysis

1. INTRODUCTION

The Infrared Space Interferometry mission[1] (IRSI) of the European Space Agency (ESA) has the objective to investigate Earth-like planets orbiting bright stars. The prospect is to detect absorption lines of potential human life indicators, like water or ozone, by spectroscopic analysis of the received planet signal in the infrared wavelength regime of 6 to 18 microns. The investigations, to be performed by an instrument positioned beyond Mars to avoid the influence of the Zodiacal Dust, are eyed on Sun/Earth-like constellations at a distance of some 50 light years (LY) from Earth.

The instrumental problems to be solved stem from the close neighbourhood of star and planet (angular separation of some $0.3\mu rad$) and from the high contrast between the two radiation sources (spectral radiance ratio of some 10^8 for a wavelength of $6\mu m$, according to Planck's law of radiation[2]). A nulling interferometer,[3] as suggested for IRSI, in principle provides both a high angular resolution to separate the planet from the star and a strong rejection of the star light. However, the required wavelength range of operation from 6 to 18 microns is a highly challenging requirement on the interferometer.

It is the aim of this paper to investigate the nulling capability of space-based nulling interferometers, realized either in fiber or bulk optics, in the presence of – stochastic – imperfections of the structure and of optical components. We discuss general aspects of nulling interferometry, including array configurations, and establish a system model describing all parameters probably influencing the rejection performance. A general mathematical model is used to analyse the star light rejection of various interferometer configurations for Sun/Earth-like constellations in the case of individual and/or combined stochastic interferometer imperfections. For one special array configuration – the Angel's Cross geometry – we show conditions and tolerance ranges which have to be met in order to achieve sufficiently large star light rejection.

For further author information:
Gusshausstrasse 25/389, A-1040 Wien, Austria
Tel.: +43-1-58801-38901
Fax: +43-1-58801-38999
e-mail: oswald.wallner@ieee.org

The Search for Extraterrestrial Intelligence (SETI) in the Optical Spectrum III, Stuart A. Kingsley, Editor, Proceedings of SPIE Vol. 4273 (2001) © 2001 SPIE · 0277-786X/01/$15.00

2. NULLING INTERFEROMETRY

Nulling interferometry is a method for separating light arriving from slightly different directions. By adjusting the phases of the signals picked up by the telescopes forming an array, destructive interference at the interferometers output is achieved for one direction of incidence while constructive interference is obtained for other directions. For the purpose in mind, the array is pointed towards the star and the spacings between the telescopes are set such that constructive interference occurs for the planet signal.

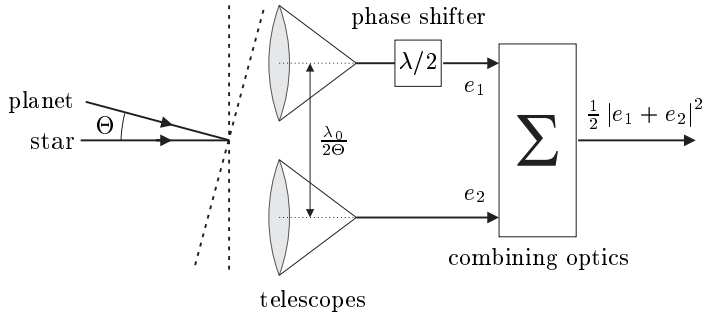

Figure 1. Principle of a nulling interferometer (e_1 and e_2 denote the optical field strengths in the interferometer arms).

In the simplest arrangement, the sum of star and planet signal incident in the observation plane are received by two identical telescopes, are then affected in phase, and finally combined to obtain an interference pattern (see Fig. 1). Destructive interference for the star signal is obtained for a relative phase shift of $\lambda/2$ between the two interferometer arms. For proper adjustment of the telescope positions, i.e. for a spacing of $\lambda_0/(2\Theta)$, the planet signal experiences full constructive interference. As the input signals are not monochromatic, the required phase relation has to be realized by an achromatic phase shifter, i.e. independent of the input signal wavelength λ. The optimum condition for telescope spacing obviously can be only fulfilled for a single wavelength, the design wavelength λ_0, which should be chosen as the lowest wavelength of the interval considered (see Sect. 4).

In practice, the interferometer will consist of an array of more than two telescopes, where the number and the geometry depend on the required rejection ratio and on the star/planet constellation. Because of the finite diameter of the star, one criterion for the rejection capability is the order of the null of the interferometer's (backpropagated) receive characteristic at the star location. The higher the order of the null, the more flat is the characteristic at the star. For good star light rejection, the large spatial extension of the star demands broad nulling, which depends on the array geometry. Figure 2 shows three exemplary telescope constellations, (a) *Bracewell*, (b) *Angel's Cross*, and (c) *Linear Bracewell*, respectively, as well as the corresponding normalized receive characteristics $G(x_s, y_s)$ – also called transmission maps. The order of the null of the Bracewell geometry is two, the one of the Angel's Cross geometry is four, and the order of the Linear Bracewell constellation is six. A star light rejection of 10^8, as it will be needed for a Sun/Earth-like constellation, requires at least an order of four.

3. SYSTEM MODEL

In order to analyse a nulling interferometer with regard to possible effects of imperfections, we established a detailed model of the system. Although an interferometer may be realized in fiber optics, in bulk optics, or in any mixture of these two, the different implementation alternatives can be treated identically if only a single spatial mode is allowed at the interferometer output. In practice this will be the case, because controlling multiple modes seems not to be realizable. Further, we considered a co-axial combining only. Multiaxial beam combining in the focal plane of a lens was ruled out because of the associated stray light.[4]

The general structure of a nulling interferometer is shown in Fig. 3. The incident radiation is coupled to the propagation medium by the *receiving unit*. The sub-beams then are affected in phase by *achromatic phase shifters*, which establish the phase relation required for star light rejection, nominally independent of the wavelength. For deep nulling, uniformity in amplitude, optical path length, and state of polarization of the signals to be combined is absolutely necessary. To this end these properties of the sub-beams are adapted by *control units*, the control signals

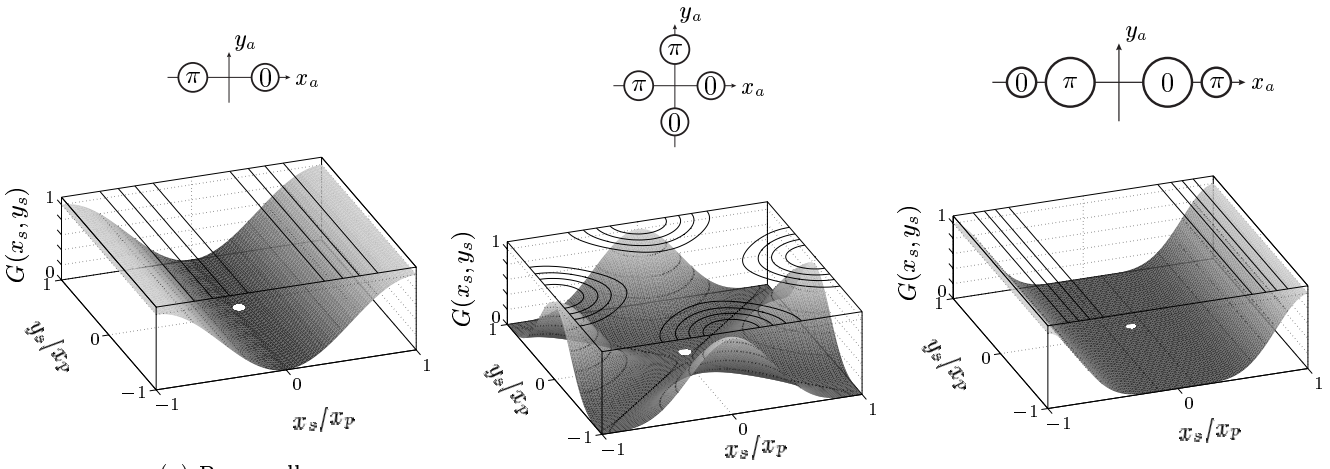

(a) Bracewell (b) Angel's Cross (c) Linear Bracewell

Figure 2. Array geometries and normalized receive characteristics $G(x_s, y_s)$ of the three exemplary interferometer configurations, (a) Bracewell, (b) Angel's Cross, and (c) Linear Bracewell. (x_s, y_s) and (x_a, y_a) are the coordinates in the source plane and the aperture plane, respectively (compare Fig. 4). (x_p, y_p) indicates the planet's position, and the quantities 0 and π indicate the phase shifts to be introduced by the achromatic phase shifters in order to reject the star light. The white circle at the centers of the receive characteristics represents the star, true to scale.

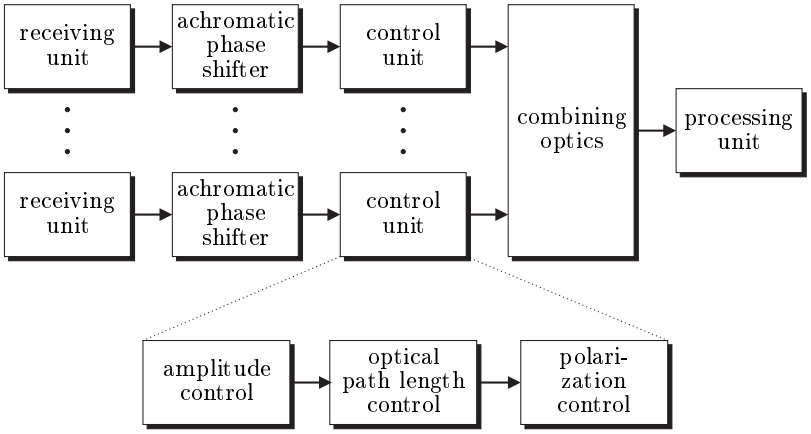

Figure 3. General structure of a nulling interferometer serving as system model.

of which are derived from the overall output signal. The *combining optics* creates the interference pattern, and in the *processing unit* the final measurement action on the output signal is performed, e.g spectroscopy of the planet signal.

If all the system components work perfectly, nulling of the star light to the theoretical limit determined by the array geometry is possible. In a practical system, imperfections of the structure and of optical components occur, leading to a reduced rejection capability.

In this paper we distinguish between two categories of imperfections: 1) Imperfections, which can be compensated by control units, like amplitude mismatch, unequal optical path lengths, or different states of polarization, respectively. 2) Imperfections and non-ideal system properties which can not be influenced by a control mechanism, like multiple reflections or waveguide dispersion. All individual errors concerning amplitude, optical path length, and state of polarization are combined to effective error values, one for each of the three parameters. This method

is applicable because only a single spatial output mode is regarded. Hence we do not analyse the influence of imperfections of individual optical components, but derive conditions the system has to fulfill as a whole.

4. MATHEMATICAL MODEL

The stellar and planetary sources are assumed to be flat, spatially incoherent Lambertian radiators located in the source plane (x_s, y_s), characterized by their spectral radiances $N_s(\lambda; x_s, y_s)$ and $N_p(\lambda; x_s, y_s)$, respectively, as given by Planck's law of radiation (see Fig. 4). Within the aperture plane (x_a, y_a), located at a distance of L $(= L_s \approx L_p)$ from the source plane, the intensities due to the two sources approximately amount to $I_s = N_s A_s \triangle\lambda / L^2$ and $I_p = N_p A_p \triangle\lambda / L^2$, respectively. The radiator's cross-sections in the source plane are denoted by A_s and A_p, and $\triangle\lambda$ is the optical bandwidth of the observer. The spectral radiances are assumed to be constant across the cross-section of each source and within the optical bandwidth. The radiation incident upon the aperture plane is collected by several telescopes, affected in amplitude, phase, and polarization, and finally superimposed co-axially to form a single output beam, which carries the optical power P_p due to the planet and P_s due to the star. As a result of the interferometer's high spatial selectivity and because of proper positioning of the telescopes and proper phasing of the subbeams, the radiation due to the star experiences destructive interference while the radiation of the planet interferes constructively. We define the interferometers rejection ratio R by

$$\frac{P_p}{P_s} = R \cdot \frac{I_p}{I_s} \quad . \tag{1}$$

The rejection ratio is the factor by which the star light is rejected when comparing the interferometer with a standard wide-field-of-view telescope.

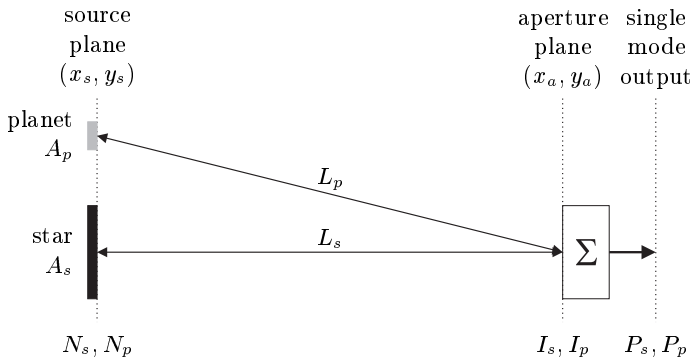

Figure 4. Geometry used for the definition of the rejection ratio.

For linearly polarized input radiation, the stochastic wave amplitude $\boldsymbol{A}$ of an N-arm single-mode interferometer of arbitrary geometry is given by the sum of the contributions $\boldsymbol{A}_n$ from the individual arms,

$$\boldsymbol{A}_n = \iint_{\mathbb{R}^2} M^*_{a,n}(x_a, y_a)\, \boldsymbol{E}_a(x_a, y_a)\, dx_a dy_a \quad , \tag{2}$$

where $\boldsymbol{E}_a$ is the stochastic optical field, and $M_{a,n}$ is the complex, normalized mode field distribution associated with arm n, both taken in the aperture plane. Since the interferometer output comprises a single spatial mode, any error in amplitude or phase transmission occurring within arm n can be taken into account by $M_{a,n}$. Applying the Van Cittert-Zernike theorem[5] to calculate the mutual intensity $\langle \boldsymbol{A}^*_m \boldsymbol{A}_n \rangle$, the average interferometer output power is given by

$$P = \langle |\boldsymbol{A}|^2 \rangle = \sum_{m=1}^{N} \sum_{n=1}^{N} \langle \boldsymbol{A}^*_m \boldsymbol{A}_n \rangle = \iint_{\mathbb{R}^2} \frac{N(\lambda; x_s, y_s)}{2} \triangle\lambda \cdot G(x_s, y_s)\, dx_s dy_s \quad , \tag{3}$$

with $N(\lambda; x_s, y_s)$ denoting the spectral radiance in the source plane and $G(x_s, y_s)$ denoting the interferometers receive characteristic backpropagated into the source plane. $G(x_s, y_s)$ is given as the squared modulus of the sum

of all normalized mode field distributions, likewise backpropagated into (x_s, y_s). The factor 1/2 is due to the fact that only a single linear state of polarisation is observed. Equation 3 shows that the average output power is the product of the radiance distribution of the source and the receive characteristic of the interferometer. Since the star is not infinitesimally small, the individual output wave contributions $\boldsymbol{A}_n$ are not perfectly correlated, i.e. $|\langle \boldsymbol{A}_m^* \boldsymbol{A}_n \rangle|^2 < \langle |\boldsymbol{A}_m|^2 \rangle \langle |\boldsymbol{A}_n|^2 \rangle$, and thus are not able to produce a perfect destructive interference, i.e. the star signal can not be perfectly rejected. The general case of unpolarized light can easily be modeled by a source emitting two orthogonal polarization modes $E_{s,x}$ and $E_{s,y}$, each being statistically independent of each other. The incident fields in the aperture plane are still statistically independent, i.e. $\langle \boldsymbol{E}_{a,x} \boldsymbol{E}_{a,y} \rangle = 0$. The derivation of the mean interferometer output power follows closely the method described before. However, since each state of polarization may be affected differently in each interferometer arm (taken into account by terms $M_{a,n,xx}$, $M_{a,n,yy}$) and even polarization crosstalk (characterized by $M_{a,n,xy}$,$M_{a,n,yx}$) may occur, the normalized mode field distribution, as introduced in Eq. 2, is a two-by-two matrix now. The average interferometer output power is given by Eq. 3, but now the receive characteristic is the sum of four different characteristics, $G = G_{xx} + G_{xy} + G_{yx} + G_{yy}$, each responsible for a certain combination of input and output state of polarization.

Equation 3 is the general expression for the mean output power of a single-mode nulling interferometer. On the basis of the assumptions mentioned in Sect. 1, several simplifications can be made to make analysis more practicable: 1) We apply a paraxial approximation. This is permissible if the lateral extensions in the source and aperture plane are much smaller than their longitudinal spacing, which is fulfilled in virtually every case. Hence, the telescope mode $M_{s,n}$ in the source plane may be expressed by the Fourier transform of the telescope mode $M_{a,n}$. 2) We assume the mode $M_{a,n}$ of telescope n to be Gaussian, characterized by mode field radius w_n, wavefront radius f_n due to subtelescope defocus, subtelescope tilts (ξ_n, η_n), and coordinates (x_n, y_n). In this case, the backpropagated telescope mode $M_{s,n}$ can be evaluated analytically. 3) The star is assumed to be a Lambertian radiator with constant spectral radiance distribution $N_s(\lambda)$ within its cross-section, a disk of radius a_s. The planet may be regarded as point source, as the variation of the receive characteristic within the planet's cross-section A_p is very small compared to the value at the planet's center (x_p, y_p). Applying these simplifications, the rejection ratio R, defined in Eq. 1, becomes

$$R = \frac{G(x_p, y_p)}{\frac{1}{a_s^2 \pi} \iint\limits_{x_s^2 + y_s^2 \le a_s^2} G(x_s, y_s)\, dx_s dy_s} \quad . \tag{4}$$

In practice, some parameters characterizing the telescope receive characteristic $G(x_s, y_s)$ exhibit stochastic variations around their optimum values. This may be due to environmental influences or due to noise induced by active control loops which are needed to achieve the required parameter conformity. To assess their influence on the rejection capability, the pertinent parameters were modeled as Gaussian random variables and the average interferometer output power due to the star and the planet was calculated. For observation times much larger than the time constant associated with the stochastic variations, the rejection ratio, Eq. 4, may be estimated by a Monte Carlo analysis, i.e. by evaluating

$$R(\lambda) = \frac{\langle \boldsymbol{G}(\lambda; x_p, y_p) \rangle}{\frac{1}{a_s^2 \pi} \iint\limits_{x_s^2 + y_s^2 \le a_s^2} \langle \boldsymbol{G}(\lambda; x_s, y_s) \rangle\, dx_s dy_s} \approx \frac{\sum_i G_i(\lambda; x_p, y_p)}{\sum_i \frac{1}{a_s^2 \pi} \iint\limits_{x_s^2 + y_s^2 \le a_s^2} G_i(\lambda; x_s, y_s)\, dx_s dy_s} \quad , \tag{5}$$

where $G_i(\lambda; x_s, y_s)$ is the receive characteristic of interferometer realisation i.

5. EXEMPLARY NUMERICAL RESULTS

To numerically analyse the influence of various imperfections on the nulling capability of interferometers we employ the general system model presented in Fig. 3. As already mentioned in Sect. 3, we combine any appearing error in amplitude or phase transmission, and any polarization mismatch to one effective error value, which is then compensated by an appropriate control unit – however, only up to a residual error as, e.g., caused by noise. Concerning the task of matching the states of polarization among the interferometer arms it is necessary to make some additional assumptions. It seems that an interferometer operating nominally in a single state of polarization is the most practicable one. Then any error in polarization is transformed to errors in amplitude and phase which may be controlled with a time constant by which the properties of the propagation medium change. Consequently we model the polarization properties of the interferometer arms as follows (compare Fig. 5): An input polarizer, characterized

by its finite, deterministic extinction ratio and by an stochastic angle, describing the mutual alignment relative to the other arms, produces a single state of polarization. For a fiber system, the (deterministic) birefringence describes the optical path length difference between the desired and the undesired polarization axis. The orientation of the fiber ends feeding the combiner are less critical and therefore assumed as deterministic quantities. At the interferometer output, a polarizer, characterized by its finite, deterministic extinction ratio, filters the nominal state of polarization.

Telescope imperfections like size or pointing mismatch cause only amplitude errors which may be compensated. Stochastic variations of the subtelescopes positions are taken into account. If the individual interferometer arms are not equal, e.g., if they are on different temperatures, dispersion will result in a wavelength-dependent behaviour of the interferometer and therefore influence the rejection performance. Just as in a Fabry-Perot structure, multiple reflections at discontinuities (e.g. fiber splices) may lead to a ripple in the optical transfer function. They decrease the nulling capability if the effect is not equal for all interferometer arms. The achromatic phase shifter and the combining optics are assumed to be ideal. Nevertheless, any error associated can be covered by one of the previous imperfections. A detailed model building the basis for the numerical analysis is shown in Fig. 5.

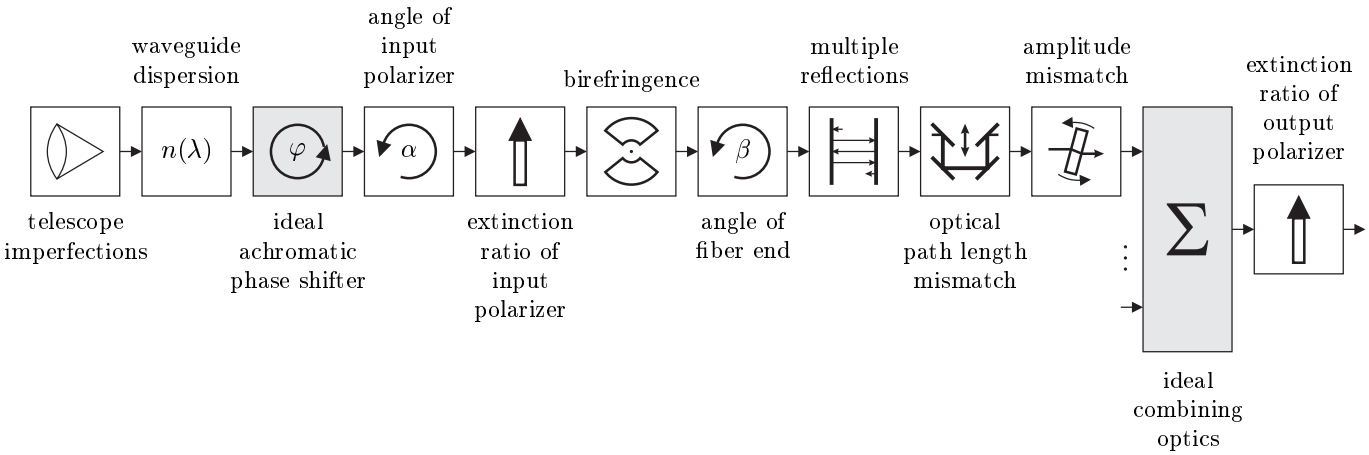

Figure 5. Simulation model of a nulling interferometer showing the imperfections considered.

In the following we discuss numerical results obtained for three array geometries with parameters as given in Tab. 1, for a Sun/Earth-like constellation as characterized in Tab. 2. Due to the wavelength dependence of the rejection ratio, it is best to optimize the array geometry for the smallest wavelength of the band to observe. The design wavelength λ_0 is the wavelength at which the first interference maximum coincides with the planet position. For $\lambda \neq \lambda_0$, the interferometers receive characteristic is scaled by a factor of λ/λ_0. For wavelengths larger than the design wavelength, the receive characteristic is broadened, resulting in an increased rejection ratio – a perfectly aligned interferometer assumed. The reason is that although the radiation due to the planet does not interfere 100% constructively, the null at the star's center becomes broader which leads to a better rejection of the star light. For wavelengths smaller than the design wavelength, the receive characteristic is compressed, which results in both a decrease of the interferometer output power due to the planet and an increase of the interferometer output power due to the star. Hence, the rejection ratio decreases rapidly (and even becomes zero if the second point of destructive interference coincides with the planet position). In the case of imperfections present, the rejection ratio also decreases by increasing wavelength.

We first analysed the influence of single imperfections on the rejection performance and then calculate the combined effect of multiple imperfections. For the statistical analysis we modeled the error of each appropriate parameter as a zero-mean, Gaussian random variable. The standard deviation σ is assumed to be equal in each interferometer arm and the individual errors are statistically independent from each other. The results shown in Figs. 6 and 7 are obtained by a Monte Carlo simulation using 1000 interferometer realisations $G_i(\lambda; x_s, y_s)$.

Figure 6 shows the estimated rejection ratio, Eq. 5, in the case of a single, zero-mean, Gaussian imperfection. The figures at the left each allow a comparison between the three exemplary interferometer configurations. The figures on the right show the wavelength dependence of the rejection ratio for the Angel's Cross geometry.

Parameter	Symbol	Bracewell		Angel's Cross				Linear Bracewell			
	$x_p x_1/(\lambda_0 L)$	1/4		1/2				1/3			
Index	n	1	2	1	2	3	4	1	2	3	4
Telescope coordinates	x_n/m	5	-5	10	-10	0	0	20/3	$-20/3$	40/3	$-40/3$
in meters	y_n/m	0	0	0	0	10	-10	0	0	0	0
Mode field radius in meters	w_n/m	1/2	1/2	1/2	1/2	1/2	1/2	1	1	1/2	1/2
Radius of wavefront curvature	f_n	$-L$									
Achromatic phase shift	φ_{APS}	0	π	0	0	π	π	0	π	π	0

Table 1. Interferometer configurations for the three exemplary array geometries. The exact telescope positions (x_n, y_n) have to be set to obtain the optimum value of $x_p x_1/(\lambda_0 L)$. The subtelescopes mode field radii w_n have deliberately been set to $0.5m$ and $1m$, respectively, and they are focussed onto the source plane by matching the focal length of the telescopes, $f_n = -L$.

Parameter	Symbol	Value	Comment
Design wavelength	λ_0	$6\mu m$	
Wavelength range	λ	$6\mu m \ldots 18\mu m$	
Star radius	a_s	$700 \cdot 10^6 m$	$\approx$ radius of Sun
Planet position	x_p	$150 \cdot 10^9 m$	$\approx$ 1 astronomical unit
	y_p	$0m$	array properly rotated
Distance star–interferometer	L	$5 \cdot 10^{17} m$	$\approx$ 50 light years

Table 2. System parameters for the numerical analysis of Sun/Earth-like constellations.

- Figures 6a and c illustrate the extraordinary requirements on optical path length and amplitude transmission uniformity. Because for Sun/Earth-like constellations a rejection ratio of some $80dB$ is required, only standard deviations of about $\sigma_p = 10^{-10}m$ for the optical path length error and $\sigma_a = 10^{-4}$ for the amplitude transmission error can be allowed. Figures 6b and d show the expected wavelength characteristic, namely an increase of R for very small errors and a decrease for large errors.

- When assessing the influence of multiple reflections at discontinuities, a single Fabry-Perot resonator with a real-valued field reflection coefficient r small compared to unity and a certain length l was assumed to be present in each interferometer arm. The field transmission is a periodic function with a period usually much smaller than the resolution bandwidth $\triangle f = \triangle\lambda\, c/\lambda^2$ of any optical spectrometer. The calculation of the rejection ratio additionally requires an integration of $G(\lambda; x_s, y_s)$ over a frequency interval determined by the resolution bandwidth.

  If the resonator lengths of the different interferometer arms differ by a quantity larger than the coherence length $(c/\triangle f)$ associated with the resolution bandwidth, the doubly-reflected optical sub-fields do not interfere with each other and effectively contribute as incoherent background (solid lines in Fig. 6f, $\triangle l = 10mm$). If the resonator lengths difference $\triangle l$ is smaller than the coherence length associated with the resolution bandwidth, the doubly-reflected sub-fields do interfere with each other and result in a rejection ratio that varies significantly with the wavelength (dashed line in Fig. 6f, $\triangle l = 10\mu m$). From Fig. 6e, one deduces that field reflection coefficients within the interferometer arms should stay well below 1% if a rejection ratio of some $80dB$ is to be achieved.

- The polarization model of the interferometer was shown in Fig. 5. The angles α of the input polarizers were modeled statistically by a standard deviation σ_α, because the pertinent tolerances are very tight and thus proper rotation of each subtelescope has to be actively maintained. Additionally, free-flying telescopes may experience strong environmental influences. As can be seen from Fig. 6g, the input polarizers main axes have to be co-aligned to within $0.1mrad$ if a rejection ratio of some $80dB$ should be achieved. The misalignment β (which lead to polarization crosstalk) of the fiber ends feeding the combiner is far less critical and will most likely not change within the observation period. Moreover, this causes only amplitude errors in the desired polarization axis, which may be compensated. Requirements on the polarizers themselves are not critical, as elements with $PXR = 60dB$ are commercially available, see Fig. 6h. The optical path length differences between the desired and the undesired polarization axes were assumed to differ by $\triangle l_p = 20\mu m$. As it can be seen in Fig. 6i, this results in a significant wavelength dependence of the rejection ratio, depending on the extinction ratio of the input polarizer.

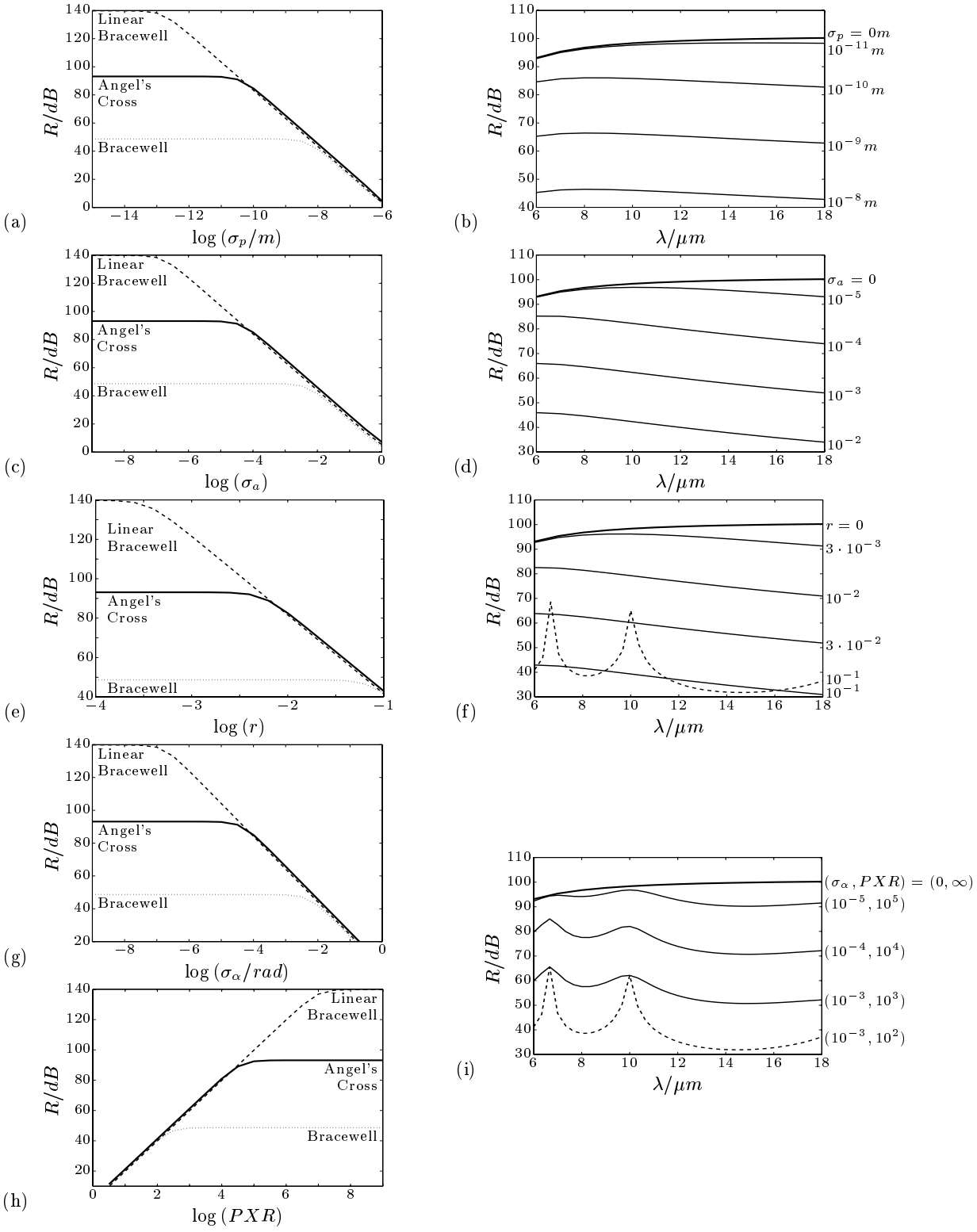

Figure 6. Rejection ratio R in the case of single imperfections present. The figures on the left show the rejection ratio of the three exemplary array configurations Bracewell, Angel's Cross, and Linear Bracewell as a function of the pertinent parameter or the standard deviation of the pertinent parameter. The figures on the right show the wavelength dependence of the rejection ratio for the Angel's Cross configuration.

If multiple imperfections are present, the rejection ratio is expected to be smaller than the smallest one caused by each imperfection separately. Figure 7 gives an example, showing the rejection ratio of the Angel's Cross interferometer configuration, due to each individual imperfection alone, and due to the combination of all imperfections for the parameters: $\sigma_p = 10^{-9}m$, $\sigma_a = 10^{-3}$, $r = \pm 10^{-2}$, $\triangle l = 10mm$, $\sigma_\alpha = 10^{-3}rad$, $PXR = 10^3$, $\triangle l_p = 20\mu m$, and $\beta = 0$.

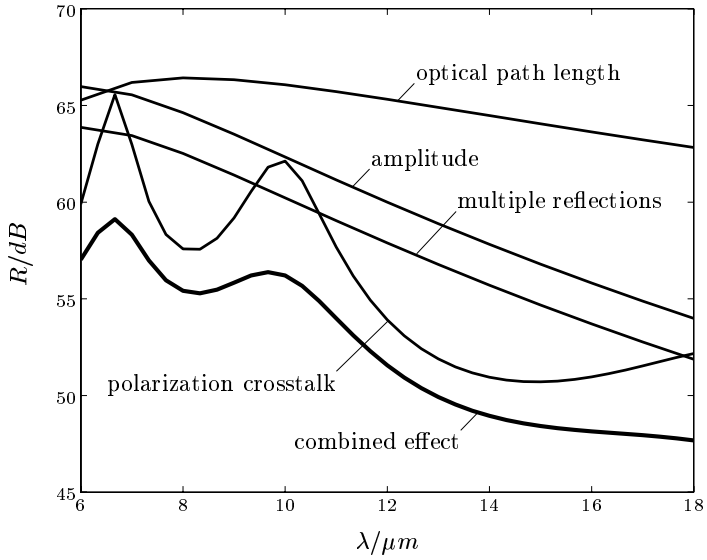

Figure 7. Rejection ratio R of the Angel's Cross interferometer as a function of the wavelength λ for the combined effects of optical path length and amplitude transmission errors, multiple reflections, and polarization crosstalk. The individual effects are also depicted.

6. ACKNOWLEDGEMENTS

The work presented in this paper was done under a contract for the European Space Agency.

REFERENCES

1. A. Léger et al., *Could We Search for Primitive Life on Extrasolar Planets in the Near Future? The DARWIN Project*, Icarus **123**, 249-255, 1996.
2. W.K. Pratt, *Laser Communication Systems*, John Wiley, New York, 1969.
3. R.N. Bracewell, R.H. McPhie, *Searching for Nonsolar Planets*, Icarus **38**, 136-147, 1979.
4. B. Mennesson, J.M. Mariotti, *Array Configurations for a Space Infrared Nulling Interferometer Dedicated to the Search for Earthlike Extrasolar Planets*, Icarus **128**, 202-212, 1997.
5. M. Born, W. Wolf, *Principles of Optics*, 7th ed., Cambridge University Press, Cambridge, 1999.